Nanoscale

PAPER

View Article Online
View Journal | View Issue

Cite this: *Nanoscale*, 2017, **9**, 802

Cross-linker mediated formation of sulfur-functionalized V_2O_5/graphene aerogels and their enhanced pseudocapacitive performance†

Gamze Yilmaz,[a,b] Xianmao Lu[c] and Ghim Wei Ho*[a,d]

Received 20th October 2016,
Accepted 1st December 2016

DOI: 10.1039/c6nr08233e

www.rsc.org/nanoscale

The development of efficient synthesis methods for the preparation of vanadium oxide (V_2O_5)–graphene holds great promise considering the excellent performance of the composite in electrochemical applications. Herein, we report the cross-linking of a V_2O_5–graphene hybrid *via* a vanadium–thiourea redox system, which allowed the assembly of graphene oxide functional groups with V_2O_5 through the reducing ability of thiourea (TU) under room conditions within an impressively short reaction time (20 min). The resulting 3D composite aerogel forms a highly porous architecture of sulfur-functionalized interconnected networks. Such sulfur-functionalized transition metal oxide–graphene-based aerogels are excellent candidates in energy storage applications. When the vanadium oxide–graphene aerogel was evaluated as an electrode for a supercapacitor, a specific capacitance as high as 484.0 F g^{-1} at 0.6 A g^{-1} was obtained in a two-electrode cell configuration. This performance is much higher than that of the vanadium oxide–graphene aerogels prepared in the absence of thiourea. The vanadium oxide–graphene aerogel is able to deliver a remarkable energy density of 43.0 Wh kg^{-1} at a power density of 0.48 kW kg^{-1} at 0.6 A g^{-1} and can hold 24.2 Wh kg^{-1} at a maximum power density of 9.3 kW kg^{-1} at 10 A g^{-1}. The symmetric supercapacitor assembled from the aerogel can retain 80% of its initial capacitance after 10 000 cycles.

1. Introduction

Nano-hybrid materials benefiting from the synergy between the unique features of the individual components are revolutionary materials in the energy-storage field for fabricating high performance supercapacitors.[1] In this context, composite structures of high power density carbon-based materials (*e.g.* graphene, carbon nanotubes, activated carbon, *etc.*) and high energy density transition metal oxides (*e.g.* RuO_2, MnO_2, Co_3O_4, NiO, Fe_2O_3, *etc.*) and sulphides have been attractive electrode candidates.[2–4] Among the commonly used carbon-based materials, graphene, a one atom-thick two-dimensional (2D) single layer of regularly packed sp^2 carbon atoms, has intriguing properties such as high thermal and electronic conductivity, excellent mechanical strength, and high specific surface area.[5,6] By assembling graphene nanosheets into graphene films and 3D graphene networks, advanced functional materials such as supercapacitor electrodes have been developed in recent years.[3] 2D graphene films have been prepared using various self-assembly methods, such as flow-directed self-assembly, layer-by-layer deposition and the Langmuir–Blodgett technique.[5] However, the irreversible restacking of graphene sheets in 2D macroscopic assemblies of graphene nanosheets, due to the strong π–π stacking interaction and van der Waals forces, results in a dramatic decrease of the accessible surface area and, therefore adversely affects mass transport and charge storage efficiency.[7,8] Alternatively, self-assembling 2D graphene sheets into highly porous and lightweight 3D interconnected graphene networks with high surface areas, such as hydrogels and aerogels, enhances the ionic and electronic transport kinetics as well as charge accommodation. Therefore, 3D interconnected graphene structures are of particular significance in energy storage applications (*e.g.*, supercapacitors and batteries). Remarkable progress has been accomplished in the self-assembly of graphene nanosheets into 3D macrostructures.[9,10] The most common strategy used for the preparation of graphene assemblies employs

[a]*Department of Electrical and Computer Engineering, National University of Singapore, 4 Engineering Drive 3, Singapore 117583, Singapore. E-mail: elehgw@nus.edu.sg*
[b]*Department of Chemical and Biomolecular Engineering, National University of Singapore, 4 Engineering Drive 4, Singapore 117585, Singapore*
[c]*Beijing Institute of Nanoenergy and Nanosystems, Chinese Academy of Sciences, China*
[d]*Engineering Science Programme, National University of Singapore, 9 Engineering Drive 1, Singapore 117575, Singapore*
†Electronic supplementary information (ESI) available. See DOI: 10.1039/c6nr08233e

physical or chemical cross-linking agents to hold 3D graphene networks together, such as sol–gel polymerization with organic molecules including biomolecules (DNA), noble-metal (Au, Ag, Pd, Ir, Rh, Pt) promoted self-assembly and divalent ion (Ca^{2+}, Ni^{2+}, Co^{+2}) driven self-assembly.[11–14] For instance, the sol–gel polymerization of resorcinol and formaldehyde with sodium carbonate as a catalyst in aqueous single-layered GO solution promotes the formation of the carbon cross-links in the graphene network.[12] Apart from the chemical or physical cross-linking based assembly, the use of a large amount of reducing agents ($NaHSO_3$, Na_2S, vitamin C, HI, and hydroquinone) has successfully prepared 3D architectures of graphene.[15,16] Although these kinds of porous graphene networks offer high power densities with excellent rate capabilities and cycling stabilities, their energy densities are limited due to the electrical-double layer charge storage mechanism. On the other hand, pseudocapacitive materials (*e.g.* transition metal oxides and conducting polymers) with multiple oxidation states possess high specific capacitances and deliver high energy densities. By combining the merits of 3D graphene networks and pseudocapacitive materials, composite electrodes exhibit enhanced performances in energy density, power density, rate capability and cycling stability. To date, a number of transition metal–oxide incorporated graphene hydrogels/aerogels, such as 3D MnO_2/graphene, $Ni(OH)_2$/graphene and Co_3O_4/graphene, have been prepared using high pressure and temperature hydrothermal treatment, generally over long reaction times.[17–19] Besides the above-mentioned transition metal oxides, vanadium pentoxide (V_2O_5) is a particularly promising candidate due to its high specific capacitance, wide potential window and earth-abundant nature.[20] A few 3D graphene/V_2O_5 aerogels have been prepared and evaluated for electrochemical applications to date.[21–23] For example, very recently, Liu *et al.* reported the formation of V_2O_5 nanoribbons on the surface of graphene sheets *via* the sol–gel process by aging HVO_3 and GO for 3 weeks.[22] Similarly, Wu *et al.* developed an approach for the *in situ* growth of V_2O_5 nanofibers in the matrix of graphene in the form of composite aerogels by a two-step successive process including the synthesis of a VO_x precursor and two-day aging of the VO_x precursor with graphene.[21] However, it remains a challenge to synthesize V_2O_5/graphene aerogels by a fast and controllable technique under mild reaction conditions.

Herein, for the first time, we report a versatile, one-step fast approach to construct a freestanding, macroscopic 3D network of V_2O_5/graphene aerogels using a vanadium–thiourea redox system. The approach leverages the chemically oxidized form of graphene, *i.e.* graphene oxide (GO) that contains rich surface functional groups, such as hydroxy, epoxide, and carboxy groups on basal planes and edges. The presence of these functional groups promotes the self-assembly of GO sheets and V_2O_5 with the assistance of thiourea (TU) as the cross-linker through the sol–gel process at room temperature within a short reaction of 20 minutes. The present strategy offers impressive advantages of simplicity, controllability, low cost and time and energy efficiency as well as *in situ* sulfurization. When the resulting lightweight and porous V_2O_5–graphene aerogels were evaluated as supercapacitor electrodes, they were able to deliver a maximum energy density of 43.0 Wh kg^{-1} at a power density of 0.48 kW kg^{-1} at 0.6 A g^{-1} and could hold 24.2 Wh kg^{-1} at a maximum power density of 9.3 kW kg^{-1} at 10 A g^{-1}.

2. Experimental

Synthesis of graphene oxide (GO)

Graphene oxide was prepared from natural graphite flakes *via* a modified Hummer's method.[24] First, 3 g of graphite flakes (Alfa Aesar, crystalline, −325 mesh), 2.5 g of $K_2S_2O_8$ (Sigma-Aldrich) and 2.5 g of P_2O_5 (Sigma-Aldrich) were successively added into 12 mL of concentrated H_2SO_4 (Merck, 95–97%). The resulting solution was then heated to 80 °C and stirred for 5 hours to get the pre-oxidized graphite. Next, it was cooled down, centrifuged and washed thoroughly with DI water (18.2 MΩ cm at 25 °C, Milli-Q) at least five times. After drying in a vacuum oven at room temperature, the pre-oxidized graphite was added into 120 mL concentrated H_2SO_4 (0 °C) and then 15 g of $KMnO_4$ (Sigma-Aldrich) was added slowly under continuous stirring. The obtained solution was heated to 35 °C and stirred for 2 h before dilution with 1000 mL of DI water. Next, 20 mL H_2O_2 (30 wt% in water, Sigma-Aldrich) was added into the diluted solution and washed with 1 L of 1 M HCl and 1 L of DI water successively. The obtained oxidized graphite powder was dried under ambient conditions in a vacuum oven. Graphite oxide with the desired concentration was prepared with DI water for further use. To ensure the removal of the unreacted acids and salts, the prepared graphite oxide solution was loaded into a dialysis cassette (Slide-A-Lyzer™ G2 Dialysis Cassettes, 10K MWCO) and floated in DI water for 1 week. DI water in the dialysis bath was changed every day to speed up the diffusion process. After dialysis, the graphite oxide was sonicated for 30 min to obtain graphene oxide.

Synthesis of vanadium pentoxide (VO) gel

Vanadium pentoxide gel was prepared by a hydrothermal reaction of V_2O_5 powder with H_2O_2. First, commercial 0.36 g V_2O_5 powder (Sigma-Aldrich) was dissolved in 30 mL DI water at room temperature under continuous stirring. Next, 5 mL of 30% H_2O_2 was added to the solution and continuously stirred for 2 hours under the same conditions. The color of the mixture changed from brown-yellow to dark red accompanied by the release of oxygen gas due to H_2O_2 dissolution. The dark-red colored homogeneous solution was transferred into a 40 mL Teflon-lined hydrothermal reaction vessel and heated at 190 °C for 15 h. The resulting brown colored V_2O_5 gel was collected upon cooling to room temperature.

Preparation of the V_2O_5/GO (VOGO) aerogel

The V_2O_5/GO (VOGO) hydrogels were prepared by mixing graphene oxide and V_2O_5 gel at the desired ratios. The obtained mixture was aged in a glass vial for ~2 weeks at room

temperature. The resulting hydrogels were washed with DI water (no dialysis) and ethanol to remove impurities. Then, they were freeze-dried overnight to obtain VOGO aerogels. For the reduction of graphene oxide, the VOGO aerogels were annealed in air at 300 °C for 3 hours with a heating rate of 10 °C min^{-1} using a muffle furnace. The reduced VOGO aerogels are referred to as 'VOG'.

Preparation of the thiourea-assisted V_2O_5/GO (VOGOS) aerogel

Thiourea-assisted hydrogels were prepared following the same procedure as un-doped hydrogels, except for the addition of thiourea as the crosslinking agent. For example, in a typical experiment for the preparation of a thiourea-assisted V_2O_5–GO aerogel (VOGOS), 5 mL V_2O_5 gel (12 mg mL^{-1}) was mixed with 5 mL aqueous GO solution (8 mg mL^{-1}) using a vortex mixer. Subsequently, 2 mL 0.9 M thiourea was added to the reaction mixture. Hydrogel formation was observed within 20 minutes. Then the as-synthesized VOGOS hydrogels were then taken out and washed with DI water and ethanol a few times, followed by freeze-drying overnight. It should be noted that dialysis was not used during the washing process of the hydrogels. For the reduction of graphene oxide, the VOGOS aerogels were annealed in air at 300 °C for 3 hours with a heating rate of 10 °C min^{-1} using a muffle furnace. The reduced VOGOS aerogels are referred to as 'VOGS'.

Materials characterization

Field emission scanning electron microscopy (FESEM) performed on a JEOL JSM-6700F was used to study the morphology of the materials. Transmission electron microscopy (TEM) and high-resolution transmission electron microscopy (HR-TEM) images were recorded by a JEOL JEM-2010 F microscope at an acceleration voltage of 200 kV. Elemental distribution was studied using energy dispersive X-ray spectroscopy (EDS) on a JEOL JSM-2100 F equipped with an Oxford/INCA EDS. Nitrogen adsorption–desorption isotherms were obtained at 77.3 K using the Autosorb-1 apparatus (Quantachrome) and pore size distribution was calculated by the BJH method based on the desorption isotherm. The atomic force microscopy (AFM) analysis was carried out on a Bruker Dimension ICON in the tapping mode. The crystal structure was obtained by X-ray diffraction (XRD) by collecting the patterns using a diffractometer (GADDS XRD system, Bruker AXS) equipped with a CuKα radiation source (λ = 1.54 Å). X-ray photoelectron spectroscopy (XPS) measurements were performed on a PHI Quantera X-ray photoelectron spectrometer with monochromated Al Kα radiation using a chamber pressure of 5×10^{-9} Torr. Fourier transform infrared (FTIR) spectroscopy was conducted on a Bio-Rad FTS-3500 ARX spectrophotometer. The Raman spectrum was obtained using a 532 nm excitation laser with a WITec Raman instrument.

Electrochemical measurements

The electrochemical properties of the samples were investigated in a two-electrode configuration at 25 °C using 1 M aqueous Na_2SO_4 solution as the electrolyte. The electrodes were prepared by pressing a homogeneous paste of 80 wt% activated material, 10 wt% carbon black (XC-72) and 10 wt% polytetrafluoroethylene (PTFE) onto a nickel foam substrate, which was followed by overnight drying at 60 °C. In two-electrode measurements, the symmetric supercapacitor devices (~2.0–3.0 mg total mass) were assembled in Swagelok-type cells using a 1 M Na_2SO_4 soaked Whatman filtration membrane as the separator. All electrochemical measurements (cyclic voltammogram (CV), galvanostatic charge–discharge (GCD) and electrical impedance spectroscopy (EIS)) were conducted on an Autolab PGSTAT302N workstation equipped with NOVA 1.10 software. The cyclic voltammograms were obtained at a potential window between 0 and 1.6 V at various scan rates. The galvanostatic charge–discharge cycles were acquired between 0 and 1.6 V at various current densities. The cycling stability tests were performed by galvanostatically charging and discharging for 10 000 consecutive cycles at 5 A g^{-1}. EIS tests were performed with a frequency loop from 10^5 Hz to 0.1 Hz by applying a sine wave with an amplitude of 5 mV at the open circuit potential.

3. Results and discussion

Three-dimensional interconnected networks of V_2O_5–graphene aerogels were prepared by a one-step, room temperature reaction using thiourea as the crosslinking agent. When thiourea is added into the V_2O_5–GO mixture, polymerization occurred instantaneously and enabled the assembly of 3D hydrogels within 20 minutes. After freeze-drying and annealing of thiourea cross-linked V_2O_5–GO hydrogels (VOGOS), vanadium oxide–graphene aerogels (VOGS) with a low density (~20.0 mg cm^{-3}) (Fig. S1†) were obtained, as presented in Fig. 1(a). The morphology of the vanadium oxide–graphene aerogels was studied by field-emission scanning electron microscopy (FESEM) and transmission electron microscopy (TEM). Fig. 1(b) and (c) present the FESEM images of the VOGS aerogels. The interior microstructure of the aerogels is composed of interconnected, randomly oriented continuous layers, resulting in a porous three-dimensional structure. Consistent with the FESEM results, TEM images show nanoribbons with a sheet-like texture sandwiched between graphene sheets (Fig. 1(d, e) and S2(b)†). The nanoribbons are several nanometers to several hundred nanometers in length and uniformly attached to the graphene surface (Fig. 1(e, f) and S2(b)†). High-resolution TEM (HRTEM) (Fig. 1(f)) further confirms the existence of a V_2O_5 nanoribbon structure on graphene by revealing an interfringe spacing of 0.38 nm which corresponds to the (002) plane of V_2O_5. For comparison, the TEM images of the as-prepared graphene oxide sheets and VOGS are presented in Fig. S2(a) and (b),† respectively. Moreover, the surface topography of the materials was characterized by atomic force microscopy (AFM). Fig. S3(a)† shows the AFM image of VOGS with the corresponding height profile. The AFM image of VOGS indicates that vanadium oxide–graphene composites are ~1 μm in length and ~30 nm in height. The vanadium oxide

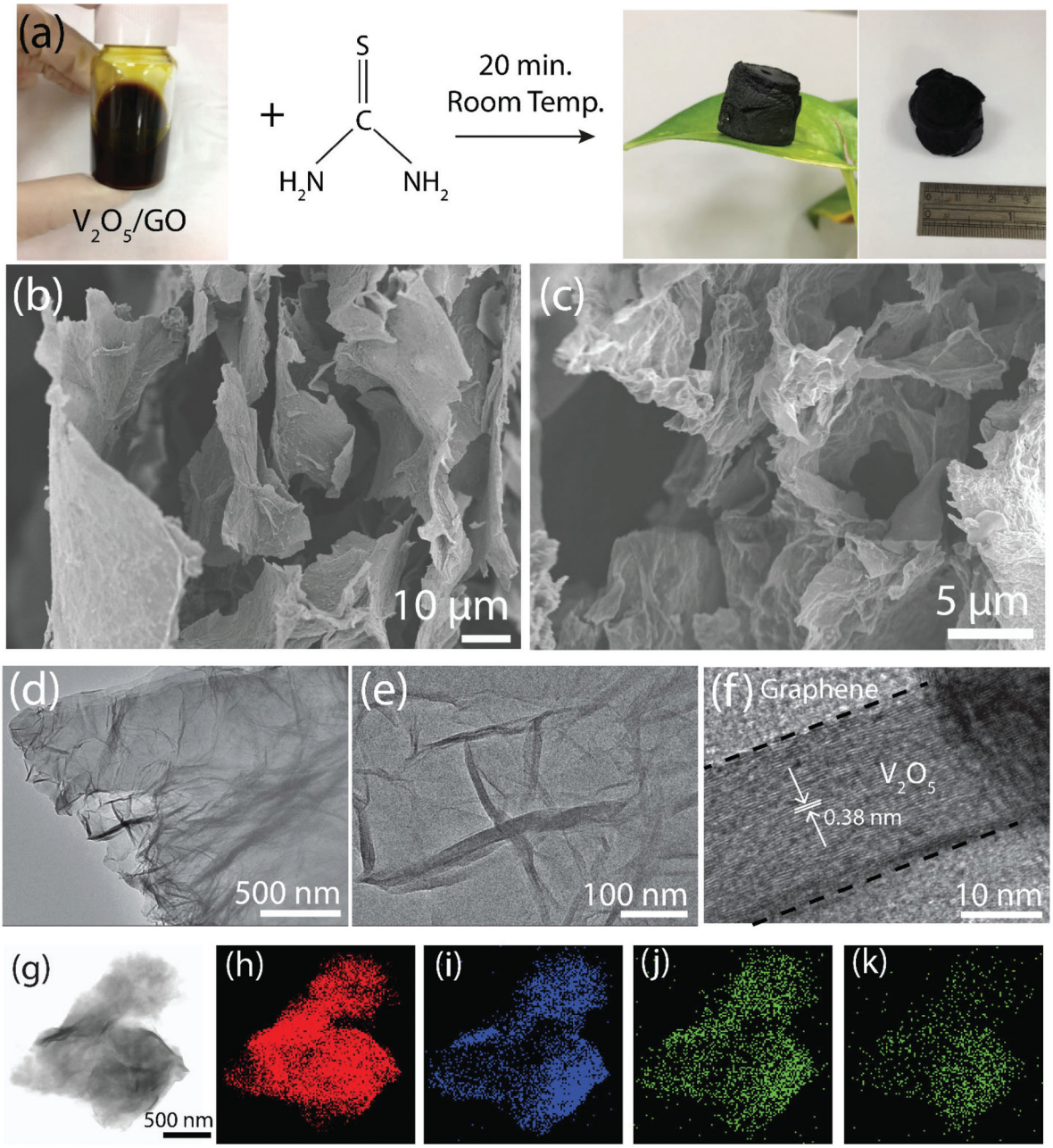

Fig. 1 (a) Digital images showing the preparation of the VOGOS hydrogel and aerogel, (b) and (c) FESEM images of the VOGS aerogel with different magnifications. (d, e) TEM and (f) HRTEM images of the VOGS aerogel. (g) STEM image of the VOGS aerogel and the corresponding element distribution mapping of (h) vanadium, (i) oxygen, (j) nitrogen and (k) sulfur.

nanoribbons decorating the graphene are not observable from the AFM images, which could be ascribed to the thin layers of V_2O_5 assembled on graphene. The nitrogen adsorption–desorption isotherm (Fig. S4†) reveals a Brunauer–Emmett–Teller (BET) surface area up to 83.4 $m^2\ g^{-1}$ with a typical mesoporous structure having a total pore volume of 0.464 $cm^3\ g^{-1}$. The uniform distribution of vanadium, oxygen, nitrogen and sulfur was further verified by energy dispersive X-ray (EDX) element mapping as shown in Fig. 1(g–k) and the atomic ratios are presented in Fig. S5.† The crystal structures of the as-synthesized graphene oxide and VOGS were identified by X-ray diffraction (XRD) (Fig. S2(c)†). Graphene oxide shows a pronounced peak at 10.0°, which is indexed to the characteristic (001) GO reflection with an interlayer distance of 8.83 Å, revealing the oxidation of graphite into monolayer graphene oxide.[25] Another peak occurring at 43° is attributed to the turbostratic band of (100) carbon materials.[26] After thermal annealing of the VOGOS aerogel at 300 °C, the corresponding XRD pattern shows a broad diffraction peak around 24.0°, which can be indexed to the (002) plane of graphene

nanosheets.[27] The corresponding interlayer spacing is larger than that of pristine graphite (3.42 Å) (Fig. S2(c)†). The remaining reflections for VOGS are attributed to orthorhombic V_2O_5 (JCPDS no. 41-1426) with a shift to higher (00l) peak positions.[28,29] Compared with VOGS, the XRD pattern of the as-synthesized VO gel (Fig. S6†) shows a series of (00l) diffraction peaks starting from the (001) reflection at 2θ = 6.18 Å. This corresponds to the $V_2O_5{\cdot}nH_2O$ (n = 2.1) structure with an interlaying spacing of 14.3 Å, which is larger than that of VOGS.[28] Similar results for the decrease in interlayer spacing with annealing have been observed, suggesting a transition from the layered to the crystalline phase due to the removal of intercalated water molecules at high temperatures.[22] The phase transition at 300 °C could be regarded as incomplete since (00l) reflections are located at higher 2θ positions than the crystalline orthorhombic V_2O_5.[22] These results indicate that the VOGS material is made of graphene sheets with mostly crystallized V_2O_5. The morphology of vanadium oxide–graphene prepared in the absence of thiourea (VOG) is presented in Fig. 2. A similar intra-structure can be observed for VOG as can be seen from Fig. 2(a). TEM images show that the architecture is composed of nanoribbons distributed over the graphene sheets. However, the EDX element mapping revealed that the distribution is not as homogeneous as in the case of VOGS (Fig. 2(c–e)). The AFM analysis further confirms that the VOG structure is covered with nanoribbons as shown in Fig. S3(b).† According to the AFM results, the V_2O_5–graphene layers in VOG are thinner than that of VOGS and V_2O_5. The assembly of graphene oxide layers *via* thiourea functioning could also contribute to the layer thickness of VOGS. This result suggests that the homogeneity of the VOGS aerogel is mainly attributable to the cross-linking function of thiourea between graphene oxide and vanadium oxide, playing a role in the formation of well-dispersed vanadium oxide–graphene structures. The overall process is illustrated in Fig. 3.

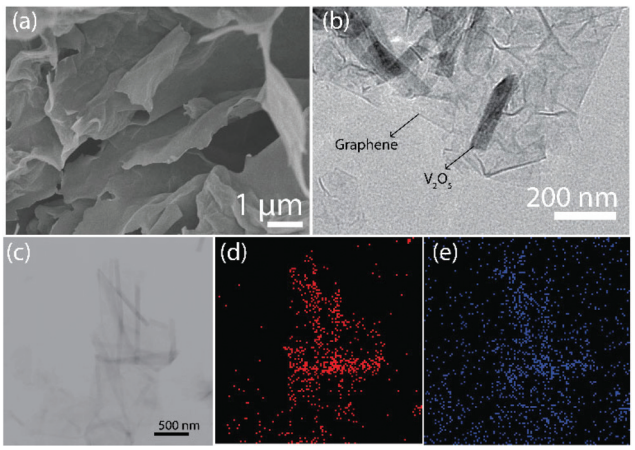

Fig. 2 (a) FESEM and (b) HRTEM images of VOG aerogel. (c) STEM image of the VOG aerogel and the corresponding element distribution mapping of (d) vanadium and (e) oxygen.

X-ray photoelectron spectroscopy (XPS) and Fourier transform infrared (FTIR) spectroscopy measurements were conducted to investigate the change in the oxidation state of the prepared materials and understand their chemical structure with a deep insight into the binding scheme after the cross-linking reaction. The V 2p XPS spectra of GO (graphene oxide), VO (vanadium oxide), VOGO (vanadium oxide–graphene oxide before annealing), VOGOS (thiourea assisted vanadium oxide–graphene oxide before annealing) and VOGS (thiourea assisted vanadium oxide–graphene after annealing) are shown in Fig. 4(a). The high-resolution V 2p spectra of all materials

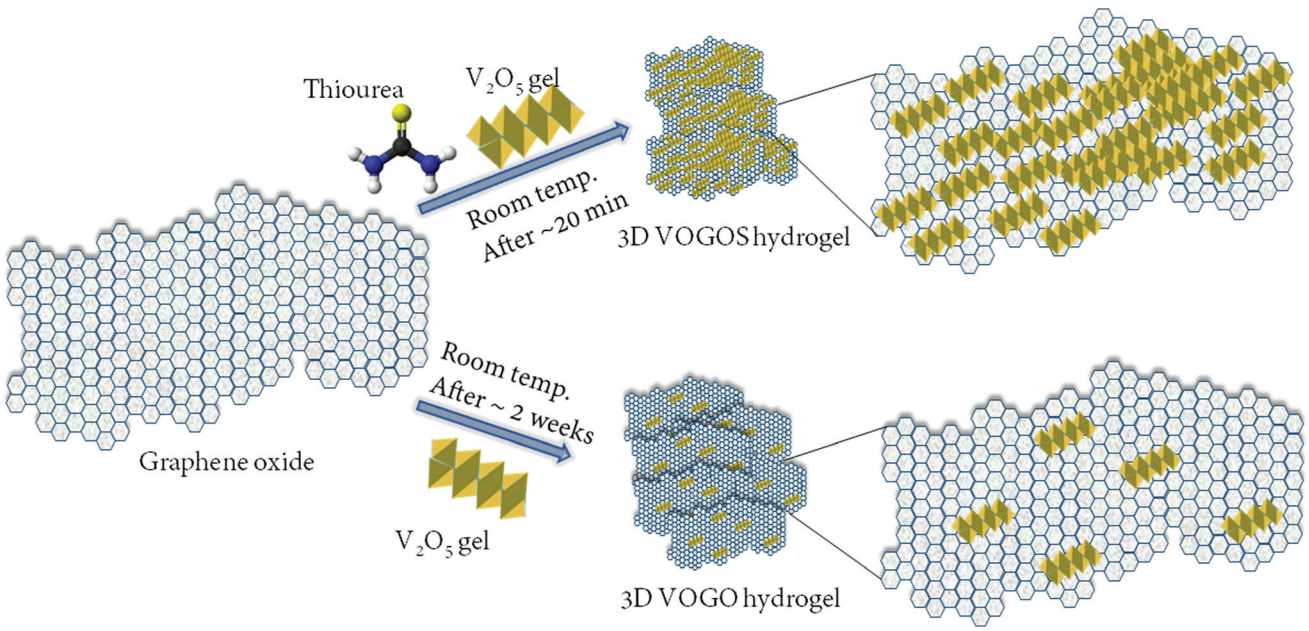

Fig. 3 Schematic illustration of the assembly process.

except VOGOS have a well-defined doublet located at 517.3 and 524.5 eV corresponding to the V $2p_{3/2}$ and V $2p_{1/2}$ core level binding energies, respectively. These binding energies agree well with the typically reported values for V^{5+} in V_2O_5.[30–32] On the other hand, VOGOS has two broad peaks; each can be deconvoluted into two binding energies. The deconvoluted V $2p_{3/2}$ (V $2p_{1/2}$) has two components with binding energies of 516.0 eV (523.3 eV) and 517.3 eV (524.5 eV) corresponding to the 4+ and 5+ oxidation states of vanadium, respectively.[32,33] The existence of V^{4+} in VOGOS implies that a portion of V^{5+} valence states was reduced to V^{4+} with the introduction of thiourea into the V_2O_5–GO system. Thiourea–V_2O_5 might be regarded as a redox couple initiating the polymerization between graphene oxide functional groups–thiourea radical–vanadium ions with the aid of the thiourea free radical produced by the interaction with V^{5+}.[34,35] Moreover, after the thermal annealing of VOGOS in air at 300 °C, the V^{4+} ion was oxidized into V^{5+} giving a final product of V_2O_5 as shown in VOGS V 2p spectra. This result was also confirmed by Raman analysis (Fig. S7†), which represents the characteristic peaks for the stretching and bending vibration modes of V_2O_5. To understand the effect of TU on the polymerization, control experiments were carried out with (1) GO–TU, (2) V_2O_5–TU and (3) V_2O_5–GO systems. Hydrogel formation was not observed for the first two systems while V_2O_5–GO (VOGO) hydrogels were formed after two weeks. This supports the key role of TU as the cross-linker. The chemical composition and functional groups of the graphene/graphene oxide containing materials were studied by the analysis of the C 1s spectra as presented in Fig. 4(b). GO spectra can be fitted into three peaks attributable to hydroxyl C–OH (287.0 eV), graphitic C–C (284.5 eV) and carboxyl O=C–OH (290.1 eV) groups.[36,37] Compared with pure graphene oxide, the graphene oxide in VOGO and VOGOS is partially reduced to graphene; since the intensity of the oxygen-containing functional groups is reduced, it suggests that graphene oxide functional groups might serve as nucleation centers for the formation of graphene–vanadium pentoxide networks. For VOGOS and VOGS, besides C–C and O=C–OH, one more peak at 285.8 eV is observed which corresponds to the C–S/C=N bonds.[38–40] To better explain the C–S and C=N binding scheme, S 2p and N 1s spectra of VOGOS were studied together with thiourea (Fig. S8†). As shown in Fig. S8(a)† the S 2p peaks of VOGOS can be resolved into three different peaks at the binding energies of 164.8, 163.6 and 168.7 eV. The former two peaks are in agreement with the reported $2p_{3/2}$ and $2p_{1/2}$ positions of sulfur connected with carbon, C–S–C, bonds.[41–44] The peak at 168.7 eV belongs to oxidized sulfur groups (C–SO_x–C, x = 2–4) such as sulfate or sulfonate. On the other hand, the TU complex showed two S 2p peaks at 162.8 and 163.8 eV which are the characteristic sulfur–carbon binding energy peaks of the TU complex.[45,46] These findings indicate the formation of a bond between graphene oxide and TU. Furthermore, the N 1s spectra of TU (Fig. S8(b)†) show a sharp peak at 399.5 eV indicating the presence of a S=C–N bond while the other N 1s peak can be ascribed to the carbon–nitrogen bonding of the thiol form due to moisture absorption.[46] These binding energies are shifted to higher values (+0.7 eV) in VOGOS compared with TU. A similar binding energy shift was previously explained for the thiourea–metal bonding which was ascribed to the increase in electron density due to the σ–π coordinated bonding with metal atoms.[46] A coordination bond can be formed between the double bonded nitrogen in thiol, a tautomeric form of thiourea in aqueous solutions, and vanadium ions. The cross-linking of TU between GO and V_2O_5 for the hydrogel complex can be constructed through sulfur or nitrogen coordination. Based on the XPS analysis, sulfur in TU could be chemically grafted to carbon in the GO functional groups and nitrogen in TU can form a bond with vanadium in V_2O_5. The proposed formation mechanism of 3D assemblies was further confirmed by FTIR studies (Fig. S9†). Based on the above characterization results and discussions, we propose a cross-linking reaction of TU with GO and V_2O_5 through chemical bonding. When the reaction mixture is composed of V_2O_5 and GO without TU, V_2O_5–GO macroscopic networks form after a long time. This might be attributed to the following reasons. In aqueous solutions, at room temperature, a large number of V^{5+} oxo-anions can form depending on the pH and vanadium concentration.[47–49] With the addition of GO to the V_2O_5 solution, the vanadium concentration decreases and the pH of the solution increases. Based on the reaction conditions of this study (pH ~ 3), decavanadic acid $[H_2V_{10}O_{28}]^{4-}$ is a possible existing molecule in the reaction mixture. This molecular form can deprotonate and form water with the carboxyl and hydroxyl groups of GO while it is also grafted on the GO. This fact can be supported by the partial reduction of GO in the

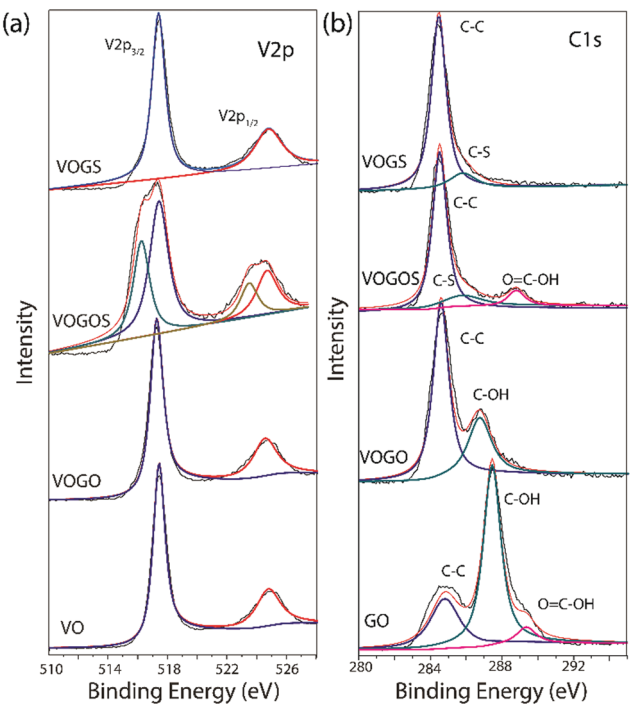

Fig. 4 (a) V 2p XPS spectra for VO, VOGO, VOGOS and VOGS. (b) C 1s XPS spectra for GO, VOGO, VOGOS and VOGS.

VOGO complex as explained above by XPS discussions and shown in C 1s XPS (Fig. 4(b)). The grafted molecule can condense and allow the formation of an oxide network. However, this is a slow process and 3D networks occur after a long time (2 weeks). These kinds of V_2O_5–GO aerogels formed with acidic vanadium species at room temperature were recently reported by Liu *et al.*[22] The 3D V_2O_5–graphene aerogel formation process was completed in 3 weeks.[22] Similarly, Wu *et al.* prepared V_2O_5–GO aerogels in 2 days using an acidic vanadium oxide precursor to initiate the condensation reactions.[21] Indeed, in our study, TU addition allowed the preparation of V_2O_5–GO aerogels in a short time (~20 minutes) under room conditions. In the TU–V_2O_5–GO system, firstly, the thiourea–vanadium oxide complex acts as a redox system to initiate the polymerization reactions.[34,35,50] The thiourea radical is produced with the reduction of V^{5+} (Fig. 4(a)). Moreover, simultaneously, the pH of the solution increases (~3.5) and vanadium concentration decreases when TU is added to the system promoting the formation of $VO(OH)_3$ precursors.[47–49] It is proposed that the reaction might be very fast since TU radicals allow the attachment of $VO(OH)_3$ precursors to the thiourea radical through nitrogen while graphene oxide is grafted to sulfur (Fig. 5). After that, the olation and oxolation reactions occur giving rise to polycondensation of the precursor and the 3D V_2O_5–graphene complex is formed.

To assess the performance of vanadium oxide–graphene aerogels for practical applications, a symmetric two-electrode cell was assembled using VOGS as both the anode and cathode material. The electrochemical measurements performed in a 1.0 M Na_2SO_4 electrolyte at an operating voltage of 0–1.6 V are shown in Fig. 6. The CV curves (Fig. 6(a)) show a symmetric and quasi-rectangular profile at high scan rates (40 and 50 mV s^{-1}) while a greater accessibility of electrolyte ions through the electrode surface at low sweep rates results in distinguishable redox peaks (5, 10, 20 and 30 mV s^{-1}). The galvanostatic charge–discharge profiles were also collected at different current densities (0.6 A g^{-1} to 10 A g^{-1}) and are presented in Fig. 6(b). The nearly linear change in voltage with time accompanied by symmetric and quasi-rectangular CV profiles indicates a good capacitive behavior with highly reversible and fast reaction kinetics. Using the CD measurements, the specific capacitance was calculated as 484.0 F g^{-1} at 0.6 A g^{-1} on the basis of the following equation: $C_{sp} = 4i\Delta t/m\Delta V$, where i is the charge–discharge current and m is the total mass of the active material including both the anode and cathode.[51,52] Fig. 6(c) and Table S1† summarize the specific and volumetric capacitance values at different current densities, respectively. The VOGS device is able to retain about 56.2% of its initial capacitance even if the current density is increased more than 10 times, which is much higher than that of the VOG

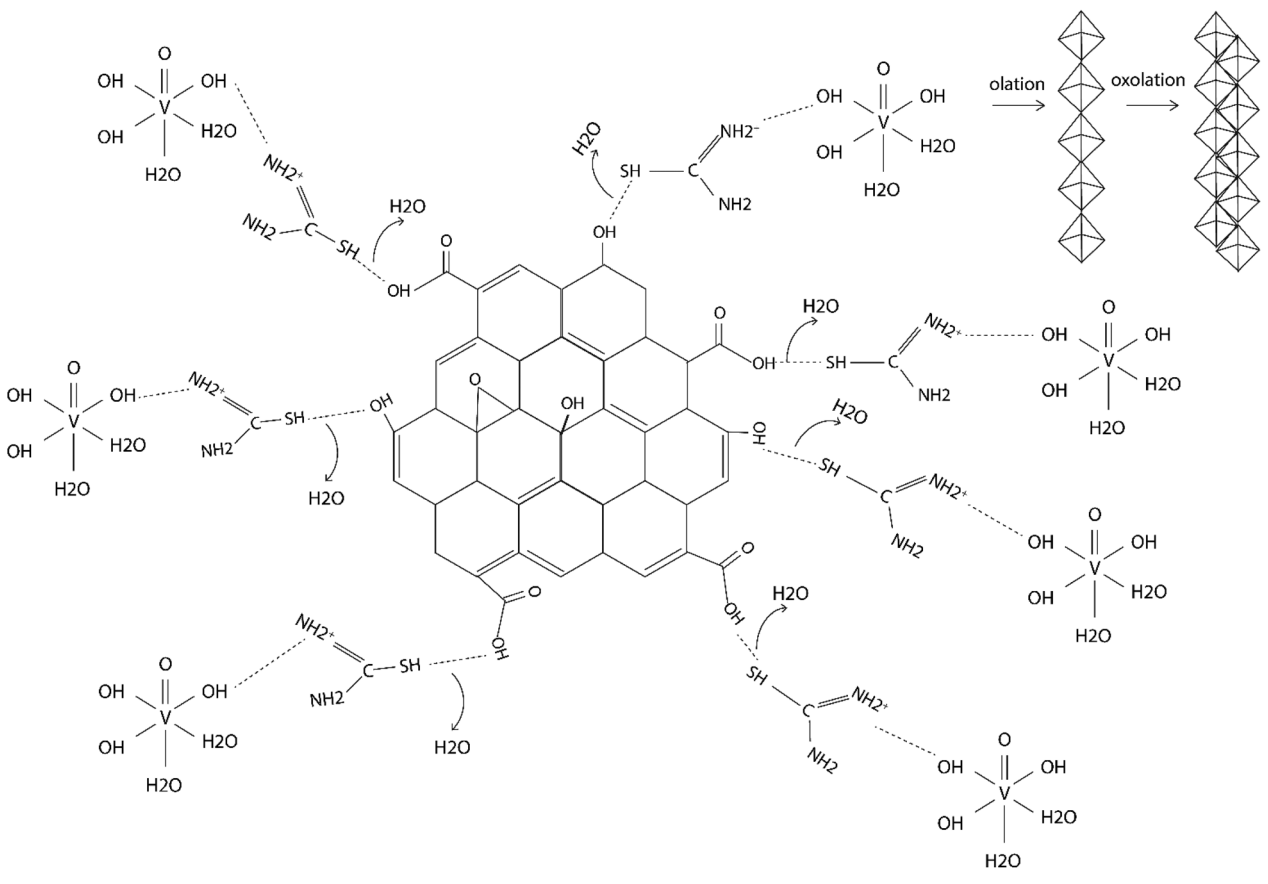

Fig. 5 Proposed reaction pathway for the formation of thiourea crosslinked VOGOS aerogels.

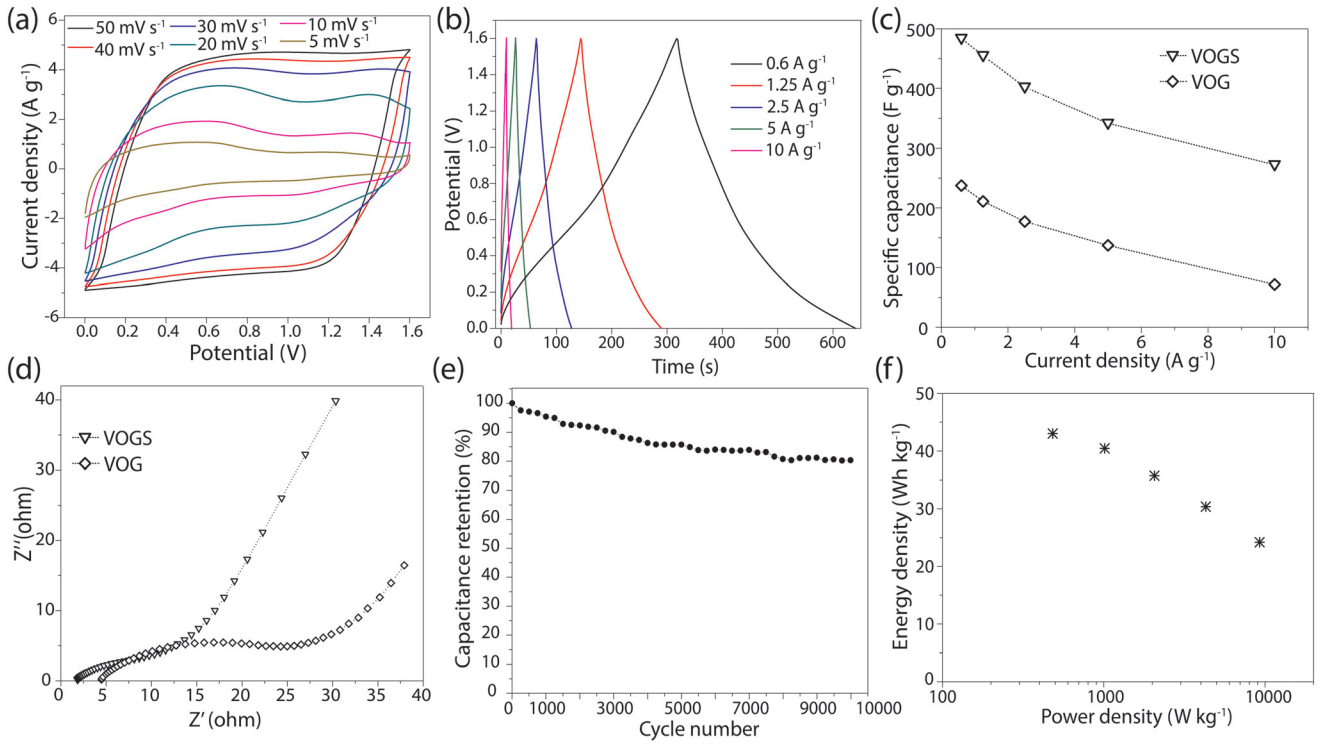

Fig. 6 (a) CV and (b) CD curves for the VOGS//VOGS device. (c) Specific capacitances obtained at different scan rates and (d) EIS performed at an open circuit potential for VOGS and VOG aerogel-based symmetric supercapacitors. (e) Cycling performance over 10 000 cycles (collected at 5 A g^{-1}) and (f) Ragone plot for the VOGS//VOGS device.

symmetric-cell. Compared with VOGS, VOG exhibits a lower specific capacitance as shown in Fig. 6(c) and S10.† To further understand the enhanced performance of the VOGS electrode, electrochemical impedance spectroscopy measurements were conducted and the corresponding Nyquist plots are presented in Fig. 6(d). The plot is composed of two characteristic regions determined by the resistances at high and low frequency regions. The semi-circle in the high frequency region is connected to a linear line in the low frequency region. The intercept of the semicircle with the real axis displays the equivalent series resistance (ESR) representing collectively the contribution of the electrolyte resistance, the contact resistance between the current collector and electrode, and the interfacial resistance between the electrolyte and electrode. The ESR of VOGS was found to be 1.6 Ω, smaller than that for VOG. Moreover, the lower charge transfer resistance of VOGS, determined from the diameter of the semi-circle, and better ion diffusion, suggested by the more vertical line, prove the better electrochemical properties of VOGS. The high performance of vanadium oxide–graphene prepared with the assistance of TU is mainly attributed to the functionalization of the aerogel with nitrogen and sulfur atoms.

Sulfur functionalized carbonaceous materials have been realized to be more attractive electrode candidates than the non-functionalized ones due to the faradaic contribution of sulfone and sulfoxide groups and their enhanced electrical conductivity.[53–56] To better clarify this phenomenon, S 2p spectra of VOGS were investigated. As can be seen from Fig. S11,† S 2p spectra exhibited two pronounced peaks at 168.5 and 169.7 eV, which were assigned to the –C–SO_x–C groups.[57–59] The sulfur-based species resulting from the annealing process provides a more polarized surface and pseudo-active sites for faradaic reactions arising from the lone electron pairs of sulfur groups undergoing redox reactions with electrolyte cations during charge/discharge processes.[53–56]

The durability of supercapacitors for long charge–discharge cycles is an important criterion for investigation of the electrochemical performance. The long-term cycling stability test was performed at 5 A g^{-1} over 10 000 consecutive charge–discharge cycles and the results are presented in Fig. 6(e). The device retains 80% of its initial capacitance after 10 000 cycles. Indeed, it can maintain 85% of the initial capacitance after the first 5000 cycles while only 5% capacitance was lost between 5000 and 10 000 cycles, revealing good long-term cycling stability. The energy density (E.D.) and power density (P.D.) of the VOGS aerogel assembled symmetric supercapacitor device were determined from the charge–discharge curves by the following equations: E.D. = $C_{sp}(\Delta V)^2/8$ and P.D. = E.D./Δt, where ΔV (V) is the operating voltage window and Δt (s) is the discharge time.[51] Fig. 6(f) shows the Ragone plot for the VOGS//VOGS device representing the energy density and power density relationship. The supercapacitor delivers a remarkable energy density of 43.0 Wh kg^{-1} at a power density of 0.48 kW kg^{-1}

at 0.6 A g^{-1} and can hold 24.2 Wh kg^{-1} at a maximum power density of 9.3 kW kg^{-1} at 10 A g^{-1}. These values are superior or comparable to most of the reported vanadium oxide-based supercapacitor devices at the same applied current density,[60–66] such as vanadium pentoxide nanofibers/graphene nanohybrids (symmetric supercapacitors with 22 Wh kg^{-1} at 0.25 A g^{-1} and asymmetric capacitors using a carbon fiber cloth as the anode with 38.8 Wh kg^{-1} at 0.5 A g^{-1}),[61,66] V_2O_5@PPy network//3D reduced graphene oxide asymmetric supercapacitors (21.0 Wh kg^{-1} at 0.25 A g^{-1}),[63] carbon coated V_2O_5 symmetric supercapacitors (10.3 Wh kg^{-1} at 1.0 A g^{-1})[64] and vanadium pentoxide//polyaniline nanofibers (26.7 Wh kg^{-1} at 0.3 A g^{-1}).[65] The notable electrochemical performance of vanadium oxide–graphene aerogel assembled supercapacitors could be attributed to their porous structure and the synergistic effect of individual materials with sulfur-enhanced capacitance.

4. Conclusions

In summary, novel 3D interconnected vanadium oxide–graphene composites were prepared by a facile and cost effective method. Thiourea functions as a cross-linker to facilitate the formation of the hybrid aerogels through chemical grafting to carbon in GO functional groups and to vanadium in V_2O_5. The assembly process allowed the homogeneous distribution of V_2O_5 on graphene nanosheets. When tested as electrode materials for supercapacitors, VOGS showed a specific capacitance as high as 484.0 F g^{-1} at 0.6 A g^{-1} in a two-electrode cell configuration. Moreover, the aerogels prepared with the aid of thiourea outperformed the ones prepared in the absence of thiourea due to a pseudocapacitive enhancement of sulfur functional groups. The VOGS//VOGS device delivers a remarkable energy density of 43.0 Wh kg^{-1} at a power density of 0.48 kW kg^{-1} and shows a long cycle life by retaining 80% of its initial capacitance after 10 000 cycles.

Notes and references

1 A. L. M. Reddy, S. R. Gowda, M. M. Shaijumon and P. M. Ajayan, *Adv. Mater.*, 2012, **24**, 5045–5064.
2 W. Wei, X. Cui, W. Chen and D. G. Ivey, *Chem. Soc. Rev.*, 2011, **40**, 1697–1721.
3 G. Wang, L. Zhang and J. Zhang, *Chem. Soc. Rev.*, 2012, **41**, 797–828.
4 T. Zhu, J. Wang and G. W. Ho, *Nano Energy*, 2015, **18**, 273–282.
5 X. Huang, X. Qi, F. Boey and H. Zhang, *Chem. Soc. Rev.*, 2012, **41**, 666–686.
6 S. Gadipelli and Z. X. Guo, *Prog. Mater. Sci.*, 2015, **69**, 1–60.
7 Z. Yan, W. Yao, L. Hu, D. Liu, C. Wang and C. S. Lee, *Nanoscale*, 2015, **7**, 5563–5577.
8 J. Luo, J. Kim and J. Huang, *Acc. Chem. Res.*, 2013, **46**, 2225–2234.
9 K. Chen, S. Song, F. Liu and D. Xue, *Chem. Soc. Rev.*, 2015, **44**, 6230–6257.
10 B. Papandrea, X. Xu, Y. Xu, C.-Y. Chen, Z. Lin, G. Wang, Y. Luo, M. Liu, Y. Huang, L. Mai and X. Duan, *Nano Res.*, 2016, **9**, 240–248.
11 Y. Xu, Q. Wu, Y. Sun, H. Bai and G. Shi, *ACS Nano*, 2010, **4**, 7358–7362.
12 M. A. Worsley, P. J. Pauzauskie, T. Y. Olson, J. Biener, J. H. Satcher Jr. and T. F. Baumann, *J. Am. Chem. Soc.*, 2010, **132**, 14067–14069.
13 X. Jiang, Y. Ma, J. Li, Q. Fan and W. Huang, *J. Phys. Chem. C*, 2010, **114**, 22462–22465.
14 Z. Tang, S. Shen, J. Zhuang and X. Wang, *Angew. Chem., Int. Ed.*, 2010, **122**, 4707–4711.
15 W. Chen and L. Yan, *Nanoscale*, 2011, **3**, 3132–3137.
16 Y. Xu, K. Sheng, C. Li and G. Shi, *ACS Nano*, 2010, **4**, 4324–4330.
17 J. Yuan, J. Zhu, H. Bi, X. Meng, S. Liang, L. Zhang and X. Wang, *Phys. Chem. Chem. Phys.*, 2013, **15**, 12940–12945.
18 S. Zhu, H. Zhang, P. Chen, L. H. Nie, C. H. Li and S. K. Li, *J. Mater. Chem. A*, 2015, **3**, 1540–1548.
19 S. Chen, J. Duan, Y. Tang and S. Zhang Qiao, *Chem. – Eur. J.*, 2013, **19**, 7118–7124.
20 G. Yilmaz, C. X. Guo and X. Lu, *ChemElectroChem*, 2016, **3**, 158–164.
21 Y. Wu, G. Gao and G. Wu, *J. Mater. Chem. A*, 2015, **3**, 1828–1832.
22 Q. Liu, Z. F. Li, Y. Liu, H. Zhang, Y. Ren, C. J. Sun, W. Lu, Y. Zhou, L. Stanciu, E. A. Stach and J. Xie, *Nat. Commun.*, 2015, **6**, 6127–6136.
23 Q. An, Y. Li, H. Deog Yoo, S. Chen, Q. Ru, L. Mai and Y. Yao, *Nano Energy*, 2015, **18**, 265–272.
24 Y. Xu, H. Bai, G. Lu, C. Li and G. Shi, *J. Am. Chem. Soc.*, 2008, **130**, 5856–5857.
25 S. H. Aboutalebi, M. M. Gudarzi, Q. B. Zheng and J. K. Kim, *Adv. Funct. Mater.*, 2011, **21**, 2978–2988.
26 L. Chen, Z. Xu, J. Li, C. Min, L. Liu, X. Song, G. Chen and X. Meng, *Mater. Lett.*, 2011, **65**, 1229–1230.
27 J. Sun, Y. Li, Q. Peng, S. Hou, D. Zou, Y. Shang, Y. Li, P. Li, Q. Du and Z. Wang, *ACS Nano*, 2013, **7**, 10225–10232.
28 W. Avansi Jr., C. Ribeiro, E. R. Leite and V. R. Mastelaro, *Cryst. Growth Des.*, 2009, **9**, 3626–3631.
29 A. V. Murugan, B. Kale, C.-W. Kwon, G. Campet and K. Vijayamohanan, *J. Mater. Chem.*, 2001, **11**, 2470–2475.
30 M. Sathiya, A. Prakash, K. Ramesha, J. M. Tarascon and A. Shukla, *J. Am. Chem. Soc.*, 2011, **133**, 16291–16299.
31 J. Zhu, L. Cao, Y. Wu, Y. Gong, Z. Liu, H. E. Hoster, Y. Zhang, S. Zhang, S. Yang and Q. Yan, *Nano Lett.*, 2013, **13**, 5408–5413.
32 G. Silversmit, D. Depla, H. Poelman, G. B. Marin and R. De Gryse, *J. Electron Spectrosc. Relat. Phenom.*, 2004, **135**, 167–175.
33 Y.-L. Ding, Y. Wen, C. Wu, P. A. van Aken, J. Maier and Y. Yu, *Nano Lett.*, 2015, **15**, 1388–1394.
34 P. L. Nayak, S. Lenka and N. C. Pati, *J. Appl. Polym. Sci.*, 1978, **22**, 3301–3309.
35 B. C. Singh, T. R. Mohanty and P. L. Nayak, *Eur. Polym. J.*, 1976, **12**, 371–376.

36 I.-Y. Jeon, Y.-R. Shin, G.-J. Sohn, H.-J. Choi, S.-Y. Bae, J. Mahmood, S.-M. Jung, J.-M. Seo, M.-J. Kim and D. W. Chang, *Proc. Natl. Acad. Sci. U. S. A.*, 2012, **109**, 5588–5593.
37 L. Peng, Z. Xu, Z. Liu, Y. Wei, H. Sun, Z. Li, X. Zhao and C. Gao, *Nat. Commun.*, 2015, **6**, 5716–5724.
38 L. Zhang, L. Ji, P.-A. Glans, Y. Zhang, J. Zhu and J. Guo, *Phys. Chem. Chem. Phys.*, 2012, **14**, 13670–13675.
39 Y. Dong, H. Pang, H. B. Yang, C. Guo, J. Shao, Y. Chi, C. M. Li and T. Yu, *Angew. Chem., Int. Ed.*, 2013, **52**, 7800–7804.
40 Z. Liu, H. Nie, Z. Yang, J. Zhang, Z. Jin, Y. Lu, Z. Xiao and S. Huang, *Nanoscale*, 2013, **5**, 3283–3288.
41 Z. Ma, S. Dou, A. Shen, L. Tao, L. Dai and S. Wang, *Angew. Chem., Int. Ed.*, 2015, **127**, 1908–1912.
42 Z. Yang, Z. Yao, G. Li, G. Fang, H. Nie, Z. Liu, X. Zhou, X. A. Chen and S. Huang, *ACS Nano*, 2011, **6**, 205–211.
43 X. Wang, Z. Zhang, X. Yan, Y. Qu, Y. Lai and J. Li, *Electrochim. Acta*, 2015, **155**, 54–60.
44 Y. Dong, S. Liu, Z. Wang, Y. Liu, Z. Zhao and J. Qiu, *Nanoscale*, 2015, **7**, 7569–7573.
45 M. Quinet, F. Lallemand, L. Ricq, J. Y. Hihn and P. Delobelle, *Surf. Coat. Technol.*, 2010, **204**, 3108–3117.
46 M. Quinet, F. Lallemand, L. Ricq, J.-Y. Hihn, P. Delobelle, C. Arnould and Z. Mekhalif, *Electrochim. Acta*, 2009, **54**, 1529–1536.
47 J. Livage, *Chem. Mater.*, 1991, **3**, 578–593.
48 O. Pelletier, P. Davidson, C. Bourgaux, C. Coulon, S. Regnault and J. Livage, *Langmuir*, 2000, **16**, 5295–5303.
49 P. Davidson, C. Bourgaux, L. Schoutteten, P. Sergot, C. Williams and J. Livage, *J. Phys. II*, 1995, **5**, 1577–1596.
50 A. Mcauley, *Coord. Chem. Rev.*, 1970, **5**, 245–273.
51 L. L. Zhang, X. Zhao, M. D. Stoller, Y. Zhu, H. Ji, S. Murali, Y. Wu, S. Perales, B. Clevenger and R. S. Ruoff, *Nano Lett.*, 2012, **12**, 1806–1812.
52 M. D. Stoller and R. S. Ruoff, *Energy Environ. Sci.*, 2010, **3**, 1294–1301.
53 W. S. V. Lee, M. Leng, M. Li, X. L. Huang and J. M. Xue, *Nano Energy*, 2015, **12**, 250–257.
54 H. N. Tien, N. T. M. Hien, E.-S. Oh, J. Chung, E. J. Kim, W. M. Choi, B. S. Kong and S. H. Hur, *J. Mater. Chem. A*, 2013, **1**, 208–211.
55 X. Zhao, Q. Zhang, C.-M. Chen, B. Zhang, S. Reiche, A. Wang, T. Zhang, R. Schlögl and D. S. Su, *Nano Energy*, 2012, **1**, 624–630.
56 Y. Huang, S. L. Candelaria, Y. Li, Z. Li, J. Tian, L. Zhang and G. Cao, *J. Power Sources*, 2014, **252**, 90–97.
57 Y. Wang, X. Li, L. Zhan, C. Li, W. Qiao and L. Ling, *Ind. Eng. Chem. Res.*, 2015, **54**, 2274–2278.
58 D. Zhang, D. Wei, W. Ding and X. Zhang, *Catal. Commun.*, 2014, **43**, 121–125.
59 D. Zhang, D. Wei, Q. Li, X. Ge, X. Guo, Z. Xie and W. Ding, *Sci. Rep.*, 2014, **4**, 4021.
60 L. Li, S. Peng, H. B. Wu, L. Yu, S. Madhavi and X. W. D. Lou, *Adv. Energy Mater.*, 2015, **5**, 1500753–1500760.
61 A. Choudhury, J. S. Bonso, M. Wunch, K. S. Yang, J. P. Ferraris and D. J. Yang, *J. Power Sources*, 2015, **287**, 283–290.
62 T. Qian, N. Xu, J. Zhou, T. Yang, X. Liu, X. Shen, J. Liang and C. Yan, *J. Mater. Chem. A*, 2015, **3**, 488–493.
63 L. Cao, J. Zhu, Y. Li, P. Xiao, Y. Zhang, S. Zhang and S. Yang, *J. Mater. Chem. A*, 2014, **2**, 13136–13142.
64 S. Balasubramanian and K. K. Purushothaman, *Electrochim. Acta*, 2015, 285–291.
65 W. F. Mak, G. Wee, V. Aravindan, N. Gupta, S. G. Mhaisalkar and S. Madhavi, *J. Electrochem. Soc.*, 2012, **159**, A1481–A1488.
66 S. D. Perera, A. D. Liyanage, N. Nijem, J. P. Ferraris, Y. J. Chabal and K. J. Balkus Jr., *J. Power Sources*, 2013, **230**, 130–137.